Vacuum Bloch–Siegert shift in Landau polaritons with ultra-high cooperativity

Xinwei Li[1], Motoaki Bamba [2,3], Qi Zhang [4], Saeed Fallahi[5], Geoff C. Gardner[5], Weilu Gao [1], Minhan Lou[1], Katsumasa Yoshioka[6], Michael J. Manfra[5,7] and Junichiro Kono [1,8,9]*

A two-level system resonantly interacting with an a.c. magnetic or electric field constitutes the physical basis of diverse phenomena and technologies. However, Schrödinger's equation for this seemingly simple system can be solved exactly only under the rotating-wave approximation, which neglects the counter-rotating field component. When the a.c. field is sufficiently strong, this approximation fails, leading to a resonance-frequency shift known as the Bloch–Siegert shift. Here, we report the vacuum Bloch–Siegert shift, which is induced by the ultra-strong coupling of matter with the counter-rotating component of the vacuum fluctuation field in a cavity. Specifically, an ultra-high-mobility two-dimensional electron gas inside a high-Q terahertz cavity in a quantizing magnetic field revealed ultra-narrow Landau polaritons, which exhibited a vacuum Bloch–Siegert shift up to 40 GHz. This shift, clearly distinguishable from the photon-field self-interaction effect, represents a unique manifestation of a strong-field phenomenon without a strong field.

An electron spin in a static magnetic field naturally precesses in a right-hand circular motion about the field axis at the Larmor frequency. For an incoming frequency-matching a.c. magnetic field, the left-hand circularly polarized (LCP) component, which rotates in the opposite direction to the spin motion, goes into and out of phase with the spin twice every oscillation period. Hence, the cumulative effect of the LCP component of the a.c. field is negligible compared with the corotating right-hand circularly polarized (RCP) component. The approach to keep only the latter component in the light–matter coupling Hamiltonian is called the rotating-wave approximation[1], which substantially simplifies the problem of calculating field–spin interactions. After the Bloch equations were generalized from the magnetic resonance context to the realm of optical resonance in two-level systems[2], the rotating-wave approximation has been ubiquitously applied to various light–matter coupling problems so successfully that, in many cases, it is implicitly made without any justification.

When the applied a.c. field becomes sufficiently strong, the rotating-wave approximation breaks down, which results in a shift in resonance frequency known as the Bloch–Siegert shift[3], stemming from interaction with the counter-rotating a.c. field component. The lowest-order term in the Bloch–Siegert shift is of the order of Ω^2/ω_0, where Ω is the Rabi frequency and ω_0 is the unperturbed resonance frequency[1]. Higher-order terms of the Bloch–Siegert shift have also been calculated quantum mechanically[4,5], which have to be taken into account to correctly estimate the magnetic moment values from magnetic resonance experiments[6]. Furthermore, recent studies on circuit quantum electrodynamics (QED) systems[7,8] have revealed frequency shifts that are equivalent to the Bloch–Siegert shift in the case of cavity QED. More recently, a Bloch–Siegert shift has been reported for a transition metal dichalcogenide system driven by circularly polarized subbandgap optical fields[9].

Here, we report a vacuum Bloch–Siegert (VBS) shift in a solid-state cavity QED system, which occurs when the average photon number inside the cavity is much less than one. The shift in this case is caused by the ultra-strong coupling (USC) of matter with the counter-rotating component of the vacuum fluctuation field inside the cavity. Such a Bloch–Siegert shift was predicted for atomic cavity QED systems[10], but an observation has been elusive due to the small dipole moments of atomic transitions. Excitations in solids are better candidates for observing a VBS shift because of the possibility of entering the USC regime, which is defined by $g/\omega_{cav} > 0.1$; here, g is the light–matter coupling rate, which is equal to half of the vacuum Rabi splitting (VRS), and ω_{cav} is the cavity photon frequency. For example, $g/\omega_{cav} = 1.43$ has been achieved using cyclotron resonance (CR) in a two-dimensional electron gas (2DEG) in semiconductor quantum wells[11]. However, no clear demonstration of a VBS shift has been made, due to the typically broad line widths caused by ultra-fast decoherence and lossy cavity designs, as well as the coexistence of competing features in the USC regime[12–14]. In the context of circuit QED, several recent studies have demonstrated USC[15–19], notably achieving $g/\omega_{cav} = 1.34$ in one study[18]. A 'quantum' Bloch–Siegert shift, similar to the VBS shift, has also been reported for a circuit QED system[15]; however, the evidence presented was based on spectral fitting with a simplified Hamiltonian that was not derived from first principles.

In our experiments, electron CR in a Landau-quantized high-mobility 2DEG in a GaAs quantum well coupled ultra-strongly with vacuum photons in a high-Q terahertz photonic crystal cavity. In this Landau polariton system, we simultaneously achieved $g/\omega_{cav} = 0.36$ and an ultra-high cooperativity $C \equiv 4g^2/\kappa\gamma = 3{,}513$, where κ and γ are the photon and matter decay rates, respectively. We found that the probe light polarization state plays a critical role in exploring USC physics in this ultra-high-cooperativity system. As shown in Fig. 1a,

[1]Department of Electrical and Computer Engineering, Rice University, Houston, TX, USA. [2]Department of Materials Engineering Science, Osaka University, Osaka, Japan. [3]PRESTO, Japan Science and Technology Agency, Saitama, Japan. [4]Argonne National Laboratories, Lemont, IL, USA. [5]Department of Physics and Astronomy, Station Q Purdue, and Birck Nanotechnology Center, Purdue University, West Lafayette, IN, USA. [6]Department of Physics, Graduate School of Engineering, Yokohama National University, Yokohama, Japan. [7]School of Materials Engineering and School of Electrical and Computer Engineering, Purdue University, West Lafayette, IN, USA. [8]Department of Material Science and NanoEngineering, Rice University, Houston, TX, USA. [9]Department of Physics and Astronomy, Rice University, Houston, TX, USA. *e-mail: kono@rice.edu
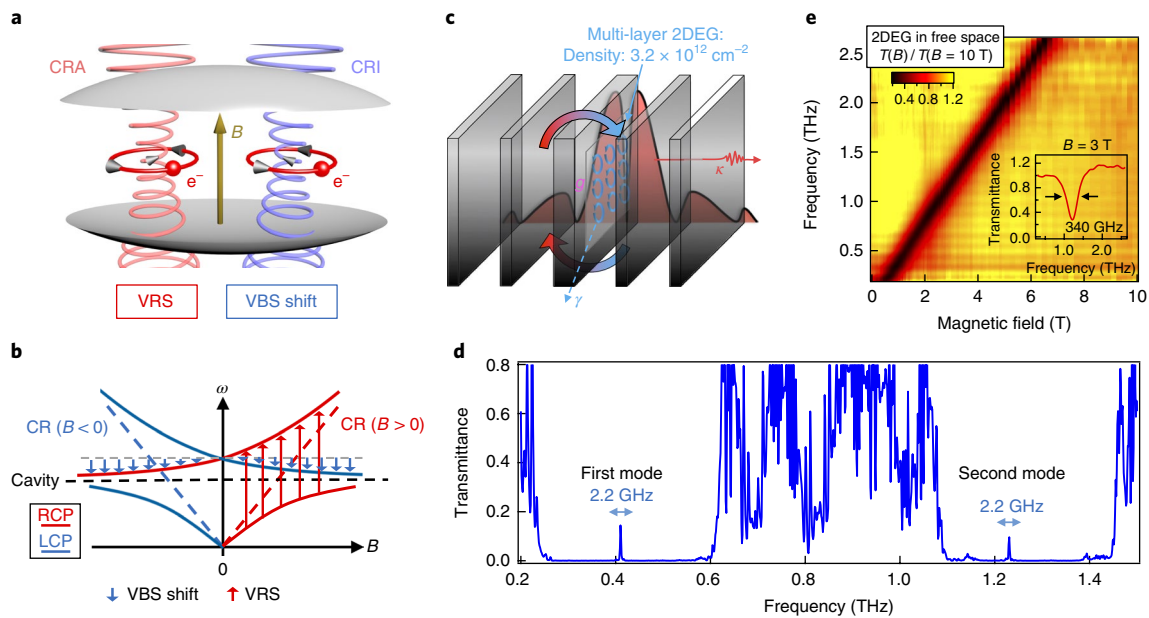
Fig. 1 | CR cavity QED setup. a, Schematic diagram for the two circularly polarized photon fields interacting with the CR of a 2DEG in a cavity. The corotating CRA mode exhibits VRS phenomena, while the counter-rotating CRI mode exhibits the VBS shift. **b**, Schematic diagram for simultaneously probing the VRS and the VBS shift in a Landau polariton system. The grey dashed line marks the upper polariton frequency at zero magnetic field. **c**, Schematic diagram for the experimental CR cavity structure. CR couples with terahertz cavity photons at coupling rate *g*. The black curve with a red shade shows the electric field intensity distribution of the first cavity mode. **d**, Transmittance spectrum for the cavity without a 2DEG, showing the first and second cavity modes with full-width at half-maximum values of 2.2 GHz and 2.4 GHz, respectively. **e**, Transmittance (*T*) spectra for the 2DEG in free space as a function of frequency and magnetic field. Inset: transmittance spectrum at 3 T, showing a CR line width of 340 GHz fit by a Lorentzian function.

the resonant corotating coupling of electrons with CR-active (CRA) circularly polarized radiation leads to the extensively studied VRS. Conversely, the counter-rotating coupling of electrons with the CR-inactive (CRI) mode leads to the time-reversed partner of the VRS, namely, the VBS shift, as we identified. Here, the separation of the VRS and the VBS shift into two time-reversed polarization states is analogous to the physics of valley-exclusive optical Stark shift and dynamical Bloch–Siegert shift observed in WS₂ (ref. [9]); see Supplementary Section 8.

Experimental scheme
Our scheme for probing the VRS and VBS shift is depicted in Fig. 1b. The energy versus magnetic field (*B*) relations measured with RCP and LCP probes are mirror symmetric about the *B* = 0 axis. Note that a negative *B* means a change in polarity compared with a positive *B*. When we use a linearly polarized terahertz probe, that is, a mixture of 50% RCP and 50% LCP radiation, in the *B* > 0 region, the RCP component shows VRS, while the VBS shift appears for the LCP component due to the state repulsion[9] between the cavity mode (black dashed line) and the CR at negative *B* fields (blue dashed line). When an RCP terahertz probe is used, one can separately observe the VRS and the VBS shift in the *B* > 0 and *B* < 0 regions, respectively. We demonstrated that the VBS shift exclusively appears in the CRI mode dispersion and is distinguished from the other unique signature of the USC regime, that is, the photon-field self-interaction effect due to the A^2 (or diamagnetic) terms, where *A* is the vector potential, in the Hamiltonian[20].

In our cavity QED setup, a 2DEG membrane containing ten GaAs quantum wells with a total electron density $n = 3.2 \times 10^{12}\,\text{cm}^{-2}$ was placed in a one-dimensional terahertz photonic crystal cavity. As shown in Fig. 1c, the cavity consisted of five silicon wafers whose thicknesses from left to right were 50 μm, 50 μm, 100 μm, 50 μm and 50 μm, respectively. Equal spacings of 195 μm were created between, forming a spatially alternating refractive index. Because the central

silicon layer was twice as thick as the other layers, it created defect cavity modes within the photonic bandgaps that would have resulted from a perfect photonic crystal structure. Figure 1d shows an experimental transmittance spectrum for a bare cavity without a 2DEG, exhibiting two sharp cavity modes with full width at half maximum of 2.2 GHz and 2.4 GHz, respectively. For each cavity mode, the electric field maximum overlapped with the 2DEG layer to ensure maximum coupling; see Fig. 1c for the electric field amplitude distribution for the first cavity mode. We varied *B* to tune the cyclotron frequency of the 2DEG, $\omega_c = eB/m^*$, where m^* is the electron effective mass and *e* is the elementary electric charge; see Fig. 1e for 2DEG magneto-transmittance spectra in free space, showing the linear evolution with *B* of a superradiance-broadened CR line[21]. The USC of CR with cavity photons occurs when ω_c is tuned to coincide with a photonic mode frequency $\omega_{\text{cav}}^{n_z}$, where n_z is the mode index.

Experimental results
Figure 2a shows linearly polarized terahertz transmittance spectra for the cavity containing the 2DEG at various *B* values in the first-order anticrossing region (around ω_{cav}^1). This experiment maps out the solid lines in the positive *B* region of Fig. 1b. Three branches of transmission peaks are well resolved in the spectra. Two of them are ascribed to the Landau polaritons arising from the CRA circularly polarized mode that resonantly coupled with CR in a corotating manner through the optical conductivity $\sigma_{\text{CRA}}(\omega) = (ne^2/m^*)/[\gamma - i(\omega - \omega_c)]$ (where ω is the terahertz angular frequency and *i* is the unit imaginary number), which has a peak at $\omega = \omega_c$. They are labelled lower polariton (LP) and upper polariton (UP), respectively, based on their frequencies. We see anticrossing of the LP and UP peaks with a large splitting, $\omega_{\text{UP}} - \omega_{\text{LP}}$, at zero detuning ($\Delta\omega = \omega_{\text{cav}}^1 - \omega_c = 0$), where ω_{UP} and ω_{LP} are UP and LP frequencies, respectively. However, the value of the coupling strength *g* is not exactly equal to $(\omega_{\text{UP}} - \omega_{\text{LP}})/2$ at $\Delta\omega = 0$, due to the coupling of CR with other photonic modes, for example, the second-order cavity mode in the photonic bandgap or transmission
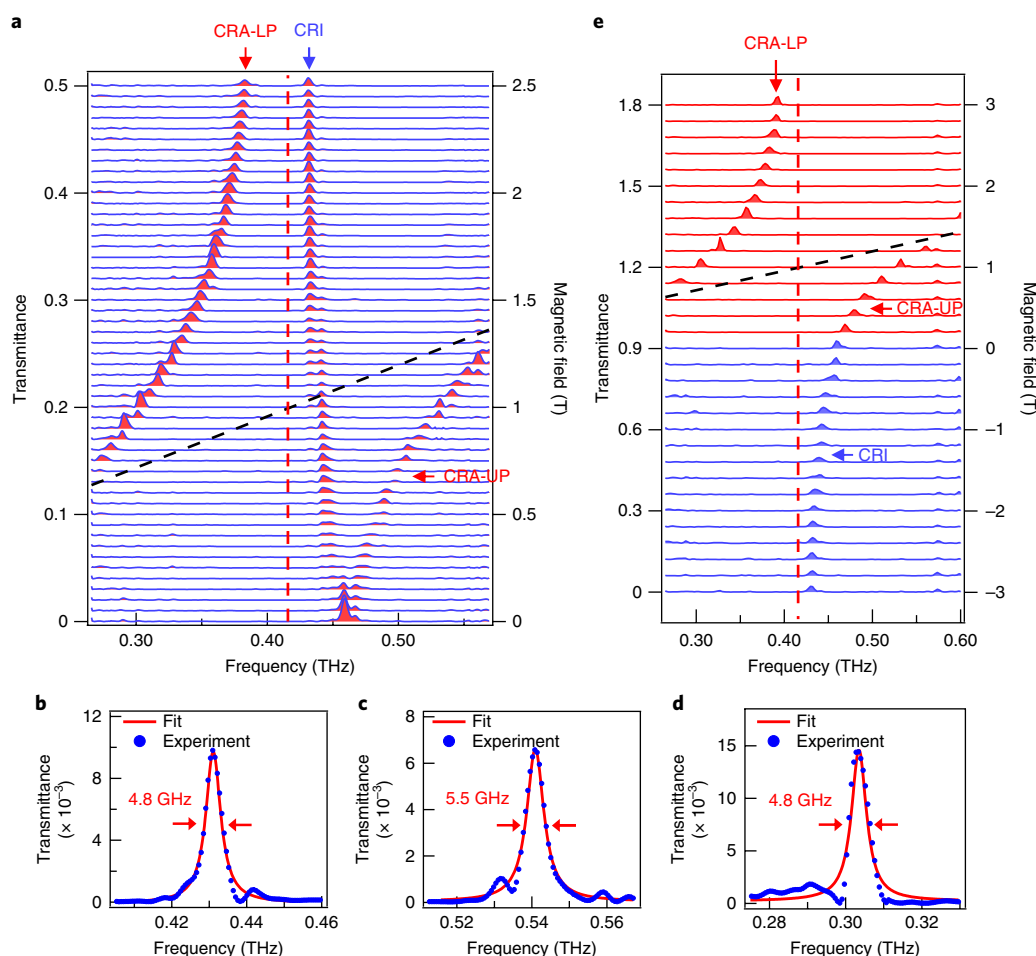
Fig. 2 | Landau polaritons in the USC regime with ultra-high cooperativity. a, Linearly polarized terahertz transmittance spectra in the B region where CR couples with the first-order cavity mode. The CRA mode splits into the LP and UP branches, exhibiting anticrossing behaviour. The CRI mode redshifts with B. The cavity mode frequency without the 2DEG (ω_{cav}^1) and the CR frequency in free space (ω_c) are shown as dashed red and black lines, respectively. **b–d**, Lorentzian fits (red line) for the CRI mode at 3 T (**b**), the UP peak at $\Delta\omega = 0$ (**c**) and the LP peak at $\Delta\omega = 0$. Experimental data points are marked by blue solid circles. (**d**). The obtained full-width at half-maximum values are indicated by the red arrows. **e**, RCP terahertz transmittance spectra in both the positive and negative B regions. The dashed red and black lines are as described in **a**.

modes in the pass bands. We determined $g/2\pi = 150.1$ GHz and $g / \omega_{cav}^1 = 0.36$ for the first-order anticrossing through theoretical estimation using device parameters (see a brief summary given below and more details in Supplementary Section 3).

The middle branch seen in Fig. 2a is the CRI circularly polarized mode, which, in free space, is not absorbed by the 2DEG, because the conductivity $\sigma_{CRI}(\omega) = (ne^2/m^*)/[\gamma - i(\omega + \omega_c)]$ does not show a peak for $\omega > 0$. However, because of USC, this mode frequency ω_{CRI} redshifts with B through counter-rotating coupling with CR. As we will show below, the shift of the CRI mode with B is the VBS shift. In the limit of an infinite B, the CRI mode and the CRA-LP converge onto the true cavity mode frequency ω_{cav}^1 of the system. The asymptotic frequency is also confirmed from the transmittance peak shown in Fig. 1d for the cavity without the 2DEG. The CRI mode closes the 'polaritonic gap' that appears in the CRA dispersion (see Supplementary Section 4); such an effect was not observed in previous studies[22,23] because the CRI mode was not probed. The mini-splitting feature observed in the CRI mode is due to back reflections from the cryostat windows; see Supplementary Section 6.

As shown in Fig. 2b–d, we determined the line widths of the CRI mode at 3 T and the UP and LP peaks at $\Delta\omega = 0$ to be 4.8 GHz, 5.5 GHz and 4.8 GHz, respectively. It was previously shown that for systems in the USC regime, UP and LP line widths are not necessarily

equal to each other[24] or simply given by $(\kappa + \gamma)/2$. In our case, as described in Supplementary Section 5, we obtained $\kappa/2\pi = 4.5$ GHz and $\gamma/2\pi = 5.7$ GHz. Here, $\kappa/2\pi$ is larger than the 2.2 GHz line width determined for a bare cavity in Fig. 1d due to the loss introduced by the 2DEG. Conversely, the intrinsic CR decay rate $\gamma/2\pi$ is 60 times smaller than the line width of CR for the same sample in free space (inset to Fig. 1e) due to the suppression of superradiance[14]. The calculated cooperativity $C = 4g^2/\kappa\gamma = 3{,}513$ is the highest reported for an intraband cavity QED system.

Figure 2e shows the transmittance spectra measured with an RCP terahertz probe. This experiment maps out the two red solid RCP lines in Fig. 1b in both the positive and the negative B regions. The RCP terahertz probe beam was generated using a terahertz achromatic quarter-wave plate[25], whose detailed characteristics are shown in Supplementary Section 7. In the positive B region, an RCP beam corresponds to the CRA mode, so we observed the CRA-UP and CRA-LP branches (red curves) that are identical to the CRA-UP and CRA-LP peaks in Fig. 2a. The CRI mode, which is absent in the positive B region, appears in the negative B region (blue curves) as an extension of the UP; however, the same RCP probe light now counter-rotates with the CR because the helicity of the electron CR motion changes. The VBS shift is again clearly observed in the CRI mode. Our RCP terahertz spectra unambiguously demonstrates

that the VRS and VBS shift are a time-reversed pair in the Landau polariton system, with distinct optical polarization selection rules.

We confirmed that Fig. 2a,e yield the same result if the CRI mode in Fig. 2a is folded about the $B = 0$ axis to the negative B region. Below, we present all the dispersion data in a way that is similar to Fig. 2e, meaning that we measured the mode frequencies with a linearly polarized probe at positive B fields, but the CRI mode was folded to the negative B region to show what we obtain when the probe is RCP. We extracted the positions of the UP, LP and CRI peaks in the first and second anticrossing regions. The dispersions are plotted in Fig. 3, together with simulation results obtained using a semiclassical transfer-matrix method with experimental material and cavity structure parameters. See Supplementary Section 2 for details on the simulations. Excellent agreement between experiment and simulation is achieved.

Theoretical analysis

We developed a quantum model, derived from the first principles (physical laws), within the electric-dipole approximation. The full Hamiltonian of the interacting CR cavity photon system is

$$\hat{H} = \hat{H}_{CR} + \hat{H}_{cav} + \hat{H}_{int} + \hat{H}_{A^2} \tag{1}$$

where $\hat{H}_{CR}$, $\hat{H}_{cav}$, $\hat{H}_{int}$ and $\hat{H}_{A^2}$ represent the Hamiltonian for the 2DEG CR, cavity photons, CR cavity photon interaction and photon-field self-interaction, respectively. These different contributions are expressed, respectively, as

$$\hat{H}_{CR} = \hbar\omega_c \hat{b}^\dagger \hat{b} \tag{2a}$$
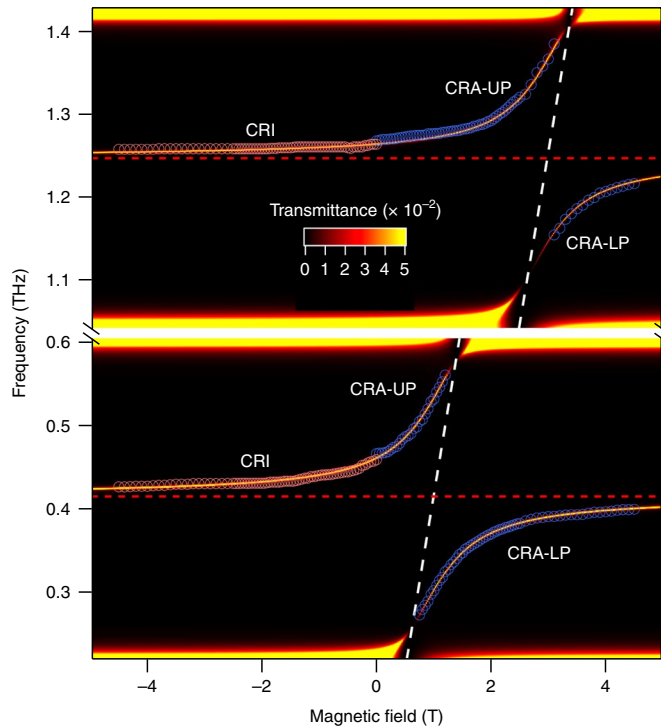

Fig. 3 | Landau polariton dispersions as a function of B. Experimental polariton peak positions (open circles) in the first and second anticrossing regions are plotted on top of a simulated transmittance colour contour map, showing excellent agreement. The cavity mode frequencies and the CR frequency in free space are shown as dashed red and white lines, respectively. The CRI mode is the CRA-UP branch in the negative B regime.

$$\hat{H}_{cav} = \sum_{n_z=1}^{\infty} \sum_{\xi=\pm} \hbar\omega_{cav}^{n_z} \hat{a}_{n_z,\xi}^\dagger \hat{a}_{n_z,\xi} \tag{2b}$$

$$\hat{H}_{int} = \sum_{n_z=1}^{\infty} i\hbar\bar{g}_{n_z} [\hat{b}^\dagger (\hat{a}_{n_z,+} + \hat{a}_{n_z,-}^\dagger) - \hat{b} (\hat{a}_{n_z,-} + \hat{a}_{n_z,+}^\dagger)] \tag{2c}$$

$$\hat{H}_{A^2} = \sum_{n_z=1}^{\infty} \sum_{n_{z'}=1}^{\infty} \frac{\hbar\bar{g}_{n_z}\bar{g}_{n_{z'}}}{\omega_c} (\hat{a}_{n_z,-} + \hat{a}_{n_z,+}^\dagger)(\hat{a}_{n_{z'},+} + \hat{a}_{n_{z'},-}^\dagger) \tag{2d}$$

where $\hbar$ is Planck's constant divided by 2π, $\hat{b}^\dagger$ ($\hat{b}$) is the creation (annihilation) operator for the collective CR excitation of the electrons in the highest Landau level, which satisfies $[\hat{b}, \hat{b}^\dagger] = 1$, $\hat{a}_{n_z,\xi}^\dagger$ ($\hat{a}_{n_z,\xi}$) represent the creation (annihilation) operator for cavity photons of the n_zth cavity mode, where ξ is the polarization index, with $+$ and $-$ representing the CRA and CRI circularly polarized modes, respectively, $\bar{g}_{n_z} = g_{n_z}\sqrt{\omega_c/\omega_{cav}^{n_z}}$ is the coupling rate of CR with the n_zth cavity mode, where $g_{n_z} = \sqrt{e^2 n/(\varepsilon_0\varepsilon_{cav}m^* L_{n_z})}$ is the coupling rate at zero detuning, L_{n_z} is the effective cavity length, ε_0 is the permittivity of free space and ε_{cav} is the relative permittivity of the cavity filling material. A detailed derivation of the Hamiltonian is given in Supplementary Section 3.

The VBS shift results from the counter-rotating coupling of CR and the cavity vacuum field. In the full Hamiltonian, equation (1), counter-rotating coupling appears in $\hat{H}_{int}$ as products of the CR operators ($\hat{b}^\dagger$ and $\hat{b}$) with the CRI mode photon operators ($\hat{a}_{n_z,-}^\dagger$ and $\hat{a}_{n_z,-}$); see equation (2c). These products are known as the counter-rotating terms (CRTs). Conversely, the terms in $\hat{H}_{A^2}$, given in equation (2d), affect both the CRA and CRI modes. When the CR photon interaction enters the USC regime, both the CRTs and the A^2 terms play non-trivial roles in the polariton physics. We found that only by measuring the CRI mode can one distinguish the CRT contribution, which exclusively leads to the VBS shift.

By solving the equations of motion of the full Hamiltonian, taking into account only the first-order cavity mode, we found that the eigen-frequencies of the CRA and CRI modes satisfy

$$\frac{\omega_{cav}^1}{\omega} = \left\{1 - \frac{2g_1^2}{\omega(\omega-\omega_c)}\right\}^{1/2} \tag{3}$$

and

$$\frac{\omega_{cav}^1}{\omega} = \left\{1 - \frac{2g_1^2}{\omega(\omega+\omega_c)}\right\}^{1/2} \tag{4}$$

respectively. Equations (3) and (4) correspond to the dispersion relations of the system; the left-hand side is proportional to k_1/ω, where $k_1 = \omega_{cav}^1\sqrt{\varepsilon_{cav}}/c$ is the confinement wavenumber and c is the speed of light in a vacuum, and the right-hand side is the effective refractive index. The B-dependent solutions to equations (3) and (4) can qualitatively reproduce essential features of the experimental CRA and CRI mode dispersions in Figs. 2a,e and 3. The positive solution to equation (4) shows a VBS shift, $\Delta\omega_{BS}$, as a function of B, whereas the solutions to equations (3) and (4) in the $B \to 0$ limit give $\omega = \sqrt{(\omega_{cav}^1)^2 + 2g_1^2}$, indicating a frequency blueshift $\Delta\omega_{A^2}(B=0) = \sqrt{(\omega_{cav}^1)^2 + 2g_1^2} - \omega_{cav}^1$ due to the A^2 terms. Note that $\Delta\omega_{A^2}(B=0)$ is known as the polaritonic gap[22,23,26]. In Supplementary

Section 3.4, we confirmed that the conclusions above are immune to photon and CR losses added to the system.

Furthermore, we simulated polariton spectra for a total of four cases, where we selectively removed the effective contributions from the CRTs and the A^2 terms from the full Hamiltonian; see Fig. 4a–d for the results plotted together with experimental data, and Supplementary Section 3 for more details. The simulation takes into account all photonic modes that are interacting with CR. From the perfect agreement between experiment and theory shown in Fig. 4a, deviations appear when either the CRTs or the A^2 terms are removed. By comparing Fig. 4a,b, we can confirm that the A^2

terms produce an overall blueshift for both polariton branches and the CRI mode. Conversely, by comparing Fig. 4a,c, we can confirm that the CRTs affect only the CRI mode, producing a VBS shift as a function of B. The shift can be quantitatively evaluated by $\Delta\omega_{BS}(B) = \omega_{CRI}(B) - \omega_{CRI}(B=0)$, where both of the CRI mode frequencies on the right are experimentally measured.

The capability of switching on and off the CRTs and the A^2 terms in the simulations allows us to determine quantitatively the experimentally observed $\Delta\omega_{BS}(B)$ and $\Delta\omega_{A^2}(B)$. As shown in Fig. 4e, in the CRI mode dispersion, $\Delta\omega_{BS}(B)$ monotonically increases with B in magnitude and reaches $-37\,$GHz at $B=5\,$T. Conversely, as
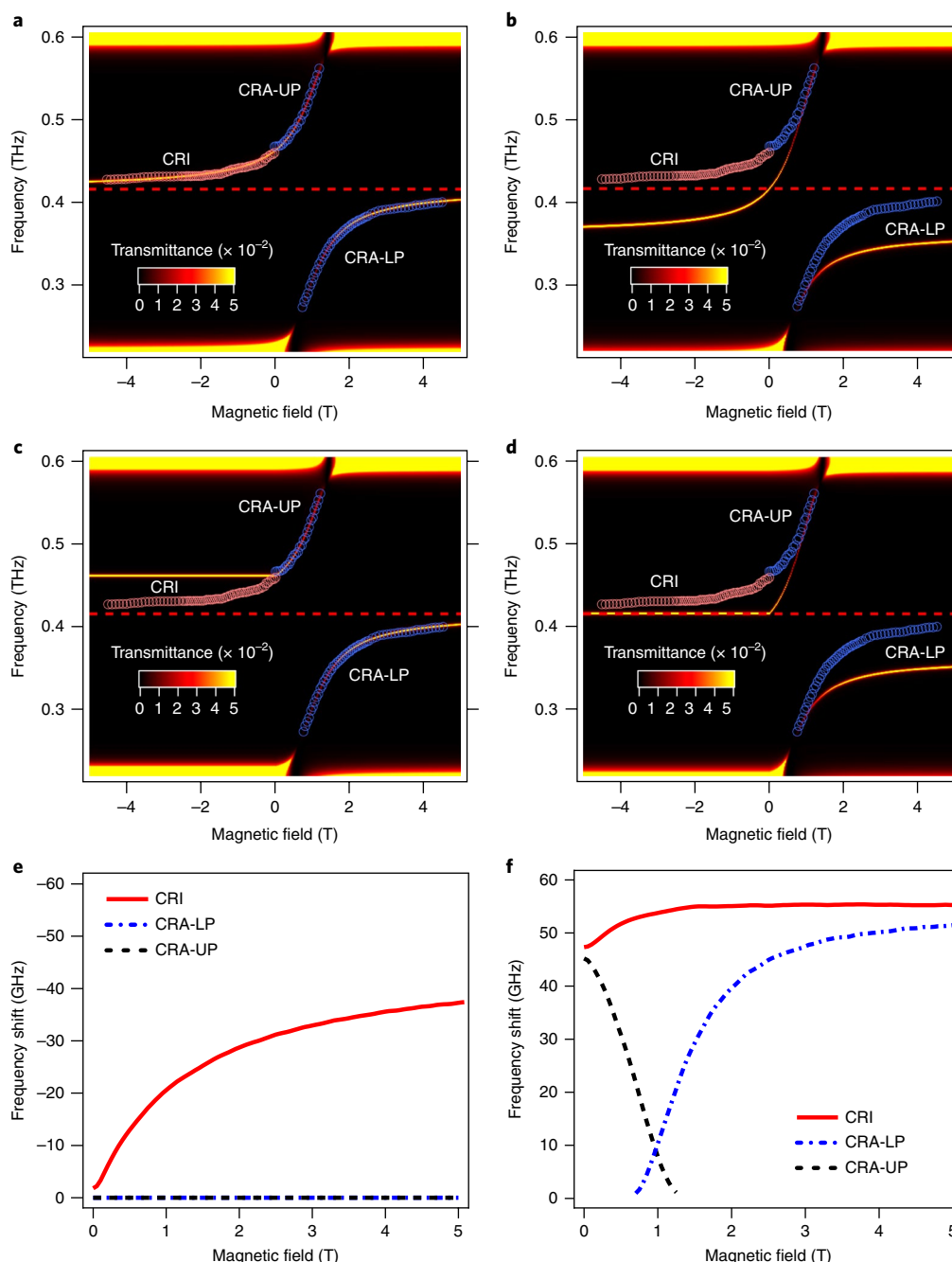

Fig. 4 | Distinction between the VBS shift due to the CRTs and the shift due to the A^2 terms in the USC regime. a–d, Simulated spectra with both the CRTs and the A^2 terms (full Hamiltonian) (**a**), with the CRTs but without the A^2 terms (**b**), without the CRTs but with the A^2 terms (**c**) and without both the CRTs and the A^2 terms (**d**). Each graph includes experimental peak positions as open circles, and the cavity mode frequency without the 2DEG (ω_{cav}^1) as the dashed red line. **e**, The VBS shift ($\Delta\omega_{BS}$) due to the CRTs as a function of B for the CRI, CRA-UP and CRA-LP peaks. **f**, The frequency shift due to the A^2 terms ($\Delta\omega_{A^2}$) as a function of B for the CRI, CRA-UP and CRA-LP peaks.

shown in Fig. 4f, both the CRA and CRI mode dispersions blueshift entirely due to the A^2 terms, leading to positive $\Delta\omega_{A^2}(B)$ shifts for all three branches. Note that $\Delta\omega_{A^2}(B)$ is larger for modes that are more photon-like, which is consistent with the fact that the A^2 terms represent the photon-field self-interaction effect. As the CRA-LP and CRA-UP branches exchange their relative weights between photon nature and CR nature as a function of B, their $\Delta\omega_{A^2}(B)$ shifts show a monotonic increase and decrease with B, respectively. The CRI mode is mainly photon-like, thus its $\Delta\omega_{A^2}(B)$ shift remains large, only slightly increasing with B.

Discussion

Our ability to determine quantitatively the separate contributions from $\Delta\omega_{BS}$ and $\Delta\omega_{A^2}$ in our experimental data is crucial for further explorations of phenomena expected to occur in the USC regime. The CRTs and A^2 terms control the realizability of many theoretical predictions. Specifically, the CRTs are crucial for producing Schrödinger-cat states[18,27] and extracavity vacuum photon emissions[28]; the A^2 terms play a decisive role in preventing the occurrence of superradiant quantum phase transitions[29–33]. Our work will thus enable quantitative evaluation of separate contributions to provide future possibilities to engineer them at will. This capability will help in the construction of best-designed quantum systems for specific applications of the phenomenon of ultra-strong light–matter coupling.

Methods

Methods, including statements of data availability and any associated accession codes and references, are available at https://doi.org/10.1038/s41566-018-0153-0.

References

1. Allen, L. & Eberly, J. H. *Optical Resonance and Two-Level Atoms* (John Wiley & Sons, New York, 1975).
2. Feynman, R. P., Vernon, F. L. & Hellwarth, R. W. Geometrical representation of the Schrödinger equation for solving maser problems. *J. Appl. Phys.* **28**, 49–52 (1957).
3. Bloch, F. & Siegert, A. Magnetic resonance for nonrotating fields. *Phys. Rev.* **57**, 522–527 (1940).
4. Shirley, J. H. Solution of the Schrödinger equation with a Hamiltonian periodic in time. *Phys. Rev.* **138**, B979–B987 (1965).
5. Cohen-Tannoudji, C., Dupont-Roc, J. & Fabre, C. A quantum calculation of the higher order terms in the Bloch-Siegert shift. *J. Phys. B* **6**, L214–L217 (1973).
6. Abragam A. *The Principles of Nuclear Magnetism* (Oxford Univ. Press, Oxford, 1961).
7. Tuorila, J. et al. Stark effect and generalized Bloch-Siegert shift in a strongly driven two-level system. *Phys. Rev. Lett.* **105**, 257003 (2010).
8. Pietikäinen, I. et al. Observation of the Bloch-Siegert shift in a driven quantum-to-classical transition. *Phys. Rev. B* **96**, 020501 (2017).
9. Sie, E. J. et al. Large, valley-exclusive Bloch-Siegert shift in monolayer WS₂. *Science* **355**, 1066–1069 (2017).
10. De Zela, F., Solano, E. & Gago, A. Micromaser without the rotating-wave approximation: the Bloch-Siegert shift and related effects. *Opt. Commun.* **142**, 106–118 (1997).
11. Bayer, A. et al. Terahertz light–matter interaction beyond unity coupling strength. *Nano. Lett.* **17**, 6340–6344 (2017).
12. Anappara, A. A. et al. Signatures of the ultrastrong light-matter coupling regime. *Phys. Rev. B* **79**(20), 201303 (R) (2009).
13. Muravev, V. M., Andreev, I. V., Kukushkin, I. V., Schmult, S. & Dietsche, W. Observation of hybrid plasmon-photon modes in microwave transmission of coplanar microresonators. *Phys. Rev. B* **83**, 075309 (2011).
14. Zhang, Q. et al. Collective non-perturbative coupling of 2D electrons with high-quality-factor terahertz cavity photons. *Nat. Phys.* **12**, 1005–1011 (2016).
15. Forn-Díaz, P. et al. Observation of the Bloch-Siegert shift in a qubit-oscillator system in the ultrastrong coupling regime. *Phys. Rev. Lett.* **105**, 237001 (2010).
16. Niemczyk, T. et al. Circuit quantum electrodynamics in the ultrastrong-coupling regime. *Nat. Phys.* **6**, 772–776 (2010).
17. Forn-Diaz, P., Romero, G., Harmans, C. J. P. M., Solano, E. & Mooij, J. E. Broken selection rule in the quantum Rabi model. *Sci. Rep.* **6**, 26720 (2016).
18. Yoshihara, F. et al. Superconducting qubit–oscillator circuit beyond the ultrastrong-coupling regime. *Nat. Phys.* **13**, 44–47 (2017).
19. Forn-Diaz, P. et al. Ultrastrong coupling of a single artificial atom to an electromagnetic continuum in the nonperturbative regime. *Nat. Phys.* **13**, 39–43 (2017).
20. Hagenmüller, D., De Liberato, S. & Ciuti, C. Ultrastrong coupling between a cavity resonator and the cyclotron transition of a two-dimensional electron gas in the case of an integer filling factor. *Phys. Rev. B* **81**, 235303 (2010).
21. Zhang, Q. et al. Superradiant decay of cyclotron resonance of two-dimensional electron gases. *Phys. Rev. Lett.* **113**, 047601 (2014).
22. Maissen, C. et al. Ultrastrong coupling in the near field of complementary split-ring resonators. *Phys. Rev. B* **90**, 205309 (2014).
23. Maissen, C., Scalari, G., Beck, M. & Faist, J. Asymmetry in polariton dispersion as function of light and matter frequencies in the ultrastrong coupling regime. *New J. Phys.* **19**, 043022 (2017).
24. Bamba, M. & Ogawa, T. System-environment coupling derived by Maxwell's boundary conditions from the weak to the ultrastrong light-matter-coupling regime. *Phys. Rev. A* **88**, 013814 (2013).
25. Kawada, Y. et al. Achromatic prism-type wave plate for broadband terahertz pulses. *Opt. Lett.* **39**, 2794–2797 (2014).
26. Scalari, G. et al. Ultrastrong coupling of the cyclotron transition of a 2D electron gas to a THz metamaterial. *Science* **335**, 1323–1326 (2012).
27. Ashhab, S. & Nori, F. Qubit-oscillator systems in the ultrastrong-coupling regime and their potential for preparing nonclassical states. *Phys. Rev. A* **81**, 042311 (2010).
28. Ciuti, C., Bastard, G. & Carusotto, I. Quantum vacuum properties of the intersubband cavity polariton field. *Phys. Rev. B* **72**, 115303 (2005).
29. Rzażewski, K., Wódkiewicz, K. & Żakowicz, W. Phase transitions, two-level atoms, and the A^2 term. *Phys. Rev. Lett.* **35**, 432–434 (1975).
30. Nataf, P. & Ciuti, C. No-go theorem for superradiant quantum phase transitions in cavity QED and counter-example in circuit QED. *Nat. Commun.* **1**, 72 (2010).
31. Bamba, M. & Ogawa, T. Stability of polarizable materials against superradiant phase transition. *Phys. Rev. A* **90**, 063825 (2014).
32. Hagenmüller, D. & Ciuti, C. Cavity QED of the graphene cyclotron transition. *Phys. Rev. Lett.* **109**, 267403 (2012).
33. Chirolli, L., Polini, M., Giovannetti, V. & MacDonald, A. H. Drude weight, cyclotron resonance, and the Dicke model of graphene cavity QED. *Phys. Rev. Lett.* **109**, 267404 (2012).

Acknowledgements

Author contributions

X.L. fabricated terahertz cavity devices, performed all measurements, analysed all experimental data and performed semiclassical simulations under the supervision and guidance of Q.Z. and J.K. M.B. performed quantum mechanical and semiclassical calculations. S.F., G.C.G. and M.J.M. grew the 2DEG sample. Q.Z., W.G., M.L. and K.Y. assisted X.L. with cavity sample preparation and measurements. X.L., M.B. and J.K. wrote the manuscript. All authors discussed the results and commented on the manuscript.

Competing interests

The authors declare no competing interests.

Additional information

Methods

Terahertz spectroscopy. We performed transmission time-domain terahertz magneto-spectroscopy measurements in the Faraday geometry. Terahertz pulses were generated from a nonlinear (110) zinc telluride crystal pumped by a Ti : sapphire-based regenerative amplifier (1 kHz, 0.9 mJ, 775 nm, 200 fs, Clark-MXR, CPA-2001) via optical rectification. Another small portion of the laser beam was split for probing terahertz radiation. The probe beam was delayed by a mechanical stage, and incident onto the detection zinc telluride crystal together with the transmitted terahertz beam for probing terahertz electric field via the electro-optic sampling method. In RCP terahertz transmittance experiments, we used an achromatic terahertz quarter-wave plate to convert the linearly polarized terahertz beam into a circularly polarized beam.

In terahertz time-domain spectroscopy, the terahertz electric field measured as a function of time can provide both amplitude and phase information. Here, for obtaining cavity transmittance spectra, we first measured a terahertz wave passing through free space as a reference, then measured under the same conditions the cavity sample. Power transmittance is defined as the square of the ratio of Fourier-transformed terahertz signal intensity spectra of the cavity sample to the reference, $T = |E_{cavity}(\omega) / E_{reference}(\omega)|^2$.

Cavity sample fabrication. To integrate the quantum-well sample with a one-dimensional terahertz photonic crystal cavity, the GaAs substrate was removed by etching. We used a mixture solution of citric acid (1 g $C_6H_8O_7$ to 1 ml deionized H_2O) and hydrogen peroxide (30% H_2O_2 and 70% H_2O by volume) to etch away the GaAs substrate until the AlAs etch-stop layer was reached. The optimized volume ratio between citric acid solution and hydrogen peroxide was 3/1. After etching, the 2.3 μm-thick quantum-well membrane was transferred onto the cavity centre defect layer and then, together with other layers, assembled into the cavity.

The sample was mounted in a liquid-helium cryostat with a variable temperature range of 1.4–300 K. A magnetic field up to 10 T was applied to the sample along the propagation direction of the incident terahertz wave (Faraday geometry).

Data availability. The data that support the plots within this paper and other findings of this study are available from the corresponding author upon reasonable request.